Two-Dimensional Compressed Correlator for Fast PN Code Acquisition

Seung-Hyun Kong, *Member, IEEE*, and Binhee Kim, *Student Member, IEEE*

***Abstract*—Acquisition of an incoming long pseudo-noise (PN) code signal requires a fast hypothesis testing function for a large number of code phase hypotheses. In addition, when a transmitter is moving at a high speed, the hypothesis testing function needs to search for the signal in a 2-Dimensional (2D) search space that includes all possible combinations of code phase hypothesis and Doppler frequency hypothesis. Since a receiver has limited hardware resources (in terms of number of correlators and computational capacity) in practice, fast PN code acquisition is not an easy goal to achieve. In this paper, we propose a double dwell search scheme, where a 2D compressed correlator (TDCC) tests a number of coherently combined neighboring code phase hypotheses and Doppler frequency hypotheses at a time in the 1st dwell search, and all individual neighboring hypotheses found in the 1st dwell search are tested in the 2nd dwell search using a conventional correlator. We present theoretical performance analysis of the proposed technique and Monte Carlo simulation results to demonstrate the performance of the proposed technique and to compare it to the conventional double dwell search technique.**

***Index Terms*—PN code acquisition, compressed correlator, compressed sensing, double dwell search.**

I. Introduction

In direct spread spectrum (DSS) systems, pseudo-noise (PN) code acquisition is a process to acquire the prompt code phase of an incoming signal, and it is the first task for a receiver to perform to initiate a communication or ranging. In some satellite communication systems and global navigation satellite systems (GNSS) using DSS signals, the PN code acquisition requires a 2-Dimensional (2D) signal search to detect the prompt PN code phase and the Doppler frequency of the incoming satellite signal [1] and [2]. For long PN code signals from low-earth orbit (LEO) satellites, the size of the 2D search space can be huge, since the lower the satellite orbit, the larger the maximum possible Doppler frequency in the incoming signal can have. In the next generation GNSS, for example, the majority of new signals employ much longer PN code sequence than the conventional civil global positioning system (GPS) signal (i.e., coarse acquisition signal). As a result, the number of total hypotheses becomes very large, and, therefore, the PN code acquisition may take a longer time or more effort for a receiver with limited amount of hardware resources than the conventional GPS receivers.

Manuscript received March 5, 2013; revised June 22, 2013; accepted August 19, 2013. The associate editor coordinating the review of this paper and approving it for publication was L. Song.

This work is supported by the National Research Foundation of Korea (NRF) grant funded by the Korean government (MEST) (No. 2011-0025867).

The authors are with the CCS Graduate School for Green Transportation, Korea Advanced Institute of Science and Technology, Taejeon, Rep. of Korea 305-701 (e-mail: skong@kaist.ac.kr). S.-H. Kong is the corresponding author.

Digital Object Identifier 10.1109/TWC.2013.092313.130407

A number of search techniques for the PN code acquisition has been introduced in the literature [1], [3]-[11]. Single dwell serial search and double dwell serial search [12] are conventional search techniques that use a correlator to test every hypothesis the the 2D search space. While mean acquisition time (MAT) for the conventional single dwell search can be large for a huge size 2D search space, techniques such as multiple dwell search [12], parallel search [13], and fast Fourier transform (FFT) based search technique [14] that performs the correlation in the frequency domain, can reduce the MAT significantly. However, the improvement (decrease) of MAT owes to the usage of dedicated hardware resources in general. For example, parallel search technique requires massive parallel correlators and FFT-based search technique uses a digital signal processor. In recent fast PN code acquisition techniques, such as folding [15] and dual folding technique [16], receiver generated PN code replica and incoming signal are folded (i.e., segmented into multiple chunks and then summed), and correlation between the generated folded PN code and the folded incoming signal is performed using the FFT-based search technique. The dual folding technique reduces the number of required correlations but has SNR degradation and requires large computational capacity for FFT. In [17], a set of parallel correlators made with a deterministic compressed sensing (DCS) matrix is introduced to reduce the number of correlators required for the parallel search technique. The DCS-based technique exploits 1D hypothesis compression (code phase hypotheses) and achieves a faster acquisition than other parallel correlators.

In this paper, we propose a double dwell search technique that employs a two-dimensional compressed correlator (TDCC) for a fast and rough estimate of PN code phase and Doppler frequency in the 1st dwell search (1st stage) and performs a fine search in the 2nd dwell search using a conventional correlator. The 2D compressed correlator (TDCC) makes use of the fact that a hypothesis testing for a code phase and Doppler frequency next to the true hypothesis can yield a non-negligible amount of signal energy. The TDCC tests a compressed hypothesis built from a set of neighboring hypotheses serially and can coherently combine the signal energy in the neighboring hypotheses to minimize SNR loss due to the combining. In TDCC, the number of total compressed hypotheses to test in the 1st stage is much smaller than the number of total individual hypotheses so that a fast and rough acquisition can be achieved. The proposed technique has much lower MAT than the conventional double dwell search, where the 1st dwell search uses a correlator with shorter correlation length than the 2nd dwell search.

The rest of this paper is organized as follows. Section II shows an algebraic analysis of the 2D signal search output, and Section III introduces the concept and algebraic analysis of the TDCC. Statistical performance analysis of the TDCC is provided in Section IV. Section V discusses practical issues regarding the employment of the TDCC such as sensitivity improvement using non-coherent accumulation, hardware complexity to implement the TDCC, and determination of the detection threshold for the fast acquisition. The performance of the proposed technique is tested with Monte Carlo simulations and a comparison to the conventional double dwell search is provided and discussed in Section VI, and, finally, conclusion is in Section VII.

II. Two-Dimensional Signal Search

Let $r(t)$ represent an incoming BPSK modulated DSS signal transmitted from a mid or low earth orbit satellite to a ground receiver, and down-converted to an intermediate frequency (IF) f_{IF}

$$r(t) = \alpha D(t-\tau)P(t-\tau)\cos(2\pi(f_{IF}+f_D)t+\theta) + n(t), \quad (1)$$

where α, $D(t)$, $P(t)$, τ, f_D, and θ represent the amplitude, data at R_b bps, PN code at R_c chip/sec (cps) ($R_c = \frac{1}{T_c} \gg R_b = \frac{1}{T_b}$), code phase, Doppler frequency, and unknown carrier phase of the incoming signal, respectively, and $n(t)$ is a complex additive white Gaussian noise (AWGN) with two-sided power spectral density $\frac{N_0}{2}$. The PN code acquisition is to find the code phase τ and the Doppler frequency f_D by searching for a correct hypothesis in a 2D search space that consists of a large number of all possible combinations of PN code phase and Doppler frequency. Since the receiver needs to find the code phase τ within a half chip ($\frac{T_c}{2}$) accuracy, the sampling rate $f_s (= \frac{1}{T_s})$ we assume is 2 times the chip rate of the PN code such that $f_s = 2R_c$.

In the conventional search techniques that use correlators, the receiver performs a correlation between the incoming signal $r(t)$ and a receiver generated signal

$$r_0(t) = P(t-\tau_l)e^{j2\pi(f_{IF}+f_D^i)t}, \quad (2)$$

where τ_l and f_D^i represent the code phase and Doppler frequency of the l-th code phase hypothesis and the i-th Doppler frequency hypothesis, respectively, being tested by the receiver. In practice, the correlation between $r(t)$ and $r_0(t)$ is carried out in the discrete-time domain. However, we use continuous-time domain expressions for the simplicity of algebraic analysis. Letting T be the length of correlation in time, and assuming $T_c \ll T \ll T_b$, the data can be considered constant during the correlation $D(u-\tau) = D$ without loss of generality, and the low-pass filtered normalized correlation output can be equivalently expressed as

$$R(\delta\tau_l, \delta f_i) = \frac{1}{T}\int_t^{t+T} h_L(u) * [r(u)r_0^*(u)]du \Big|_{t=t_0} \quad (3a)$$

$$\simeq \frac{\alpha D}{T}\int_{t_0}^{t_0+T} P(u)P(u-\delta\tau)e^{j(2\pi\delta f_i u+\theta)} + n(t)P(u-\tau_l)e^{-j(2\pi(f_{IF}+f_D^i)u)}du, \quad (3b)$$

where $h_L(t)$ is a low-pass filter, t_0 is the time when the correlation in (3a) starts. The $h_L(t)$ filters out signal components with high frequencies (e.g., $2f_{IF}+f_D+f_D^i$), and the output of the high frequency signal components is negligible in (3a). As a result, the expression in (3a) can be approximated by (3b). The quantity $R(\delta\tau_l, \delta f_i)$ depends on both code phase difference $\delta\tau_l = \tau - \tau_l$ and Doppler frequency difference $\delta f_i = f_D - f_D^i$. In noiseless case, $R(\delta\tau_l, \delta f_i)$ can be expressed as follows.

$$\frac{1}{T}\int_{t_0}^{t_0+T} P(u-\tau)P(u-\tau_l)e^{j(2\pi\delta f_i u+\theta)}du \quad (4a)$$

$$= \sum_{m=0}^{\frac{T}{T_c}-1}\Bigg[\int_{t_0+T_c m}^{t_0+T_c(m+1)-|\delta\tau_l|} e^{j(2\pi\delta f_i u+\theta)}du + \int_{t_0+T_c(m+1)-|\delta\tau_l|}^{t_0+T_c(m+1)} P(u)P(u-\delta\tau_l)e^{j(2\pi\delta f_i u+\theta)}du\Bigg] \quad (4b)$$

$$\simeq \frac{\sin(\pi\delta f_i T)}{\pi\delta f_i T}\times e^{j(2\pi\delta f_i t_0+\theta)}\times e^{j(\pi\delta f_i T)} \times e^{-j(\pi\delta f_i|\delta\tau_l|)}\times\frac{\sin(\pi\delta f_i(T_c-|\delta\tau_l|))}{\sin(\pi\delta f_i T_c)} \quad (4c)$$

The boundary of the second integral in (4b) indicates that $P(u)$ and $P(u-\tau_l)$ are completely independent, so that the second integral in (4b) can be negligible, and the approximate expression in (4c) can be obtained. Fig. 1 shows the numerically evaluated magnitudes of (4a) and (4c) with $t_0 = 0$. From (4c), $R(\delta\tau_l, 0)$ is the auto-correlation function (ACF) output

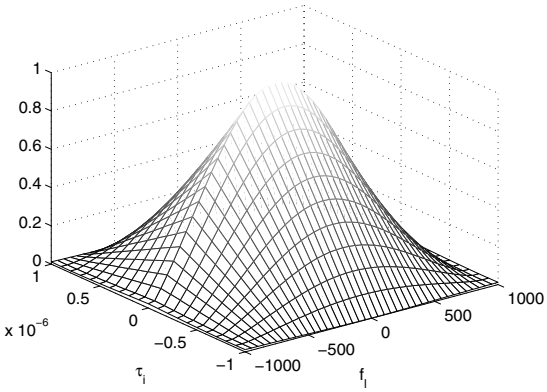

(a) Simulated ACF output using (4a)

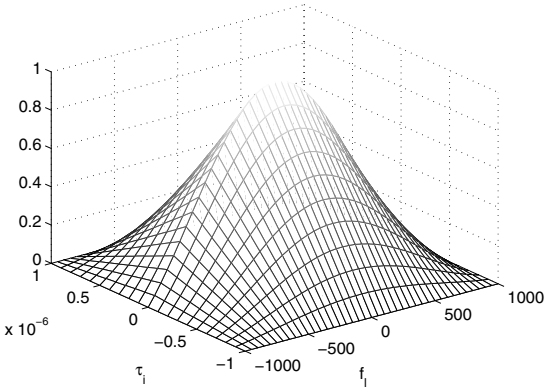

(b) Modeled ACF output in (4c)

Fig. 1. Magnitude of auto correlation output.

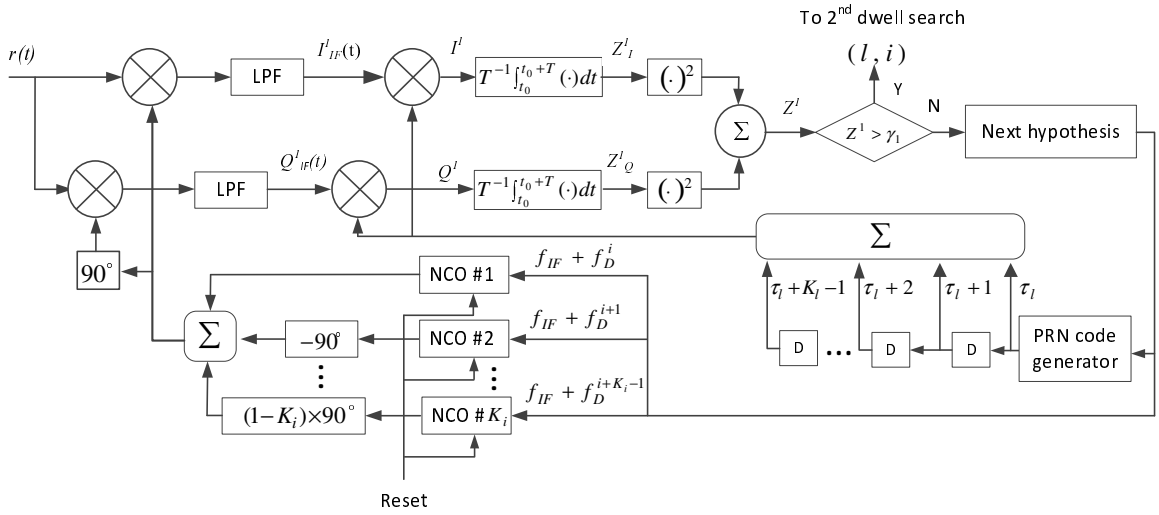

Fig. 2. 2-dimensional compressed correlator for the 1st dwell search.

of the PN code

$$R(\delta\tau_l,0)\simeq\begin{cases}(1-\dfrac{|\delta\tau_l|}{T_c})T, & |\delta\tau_l|\le T_c\\ 0, & \text{otherwise,}\end{cases}\tag{5}$$

and that $R(0,\delta f_i)$ represents the correlation result due to a Doppler frequency error. From (5), there are three consecutive code phase hypotheses that can yield non-negligible signal energy for a receiver with $f_s=2R_c$, and from (4c),

$$R(0,\delta f_i)=e^{j(2\pi\delta f_i t_0+\theta)}\times e^{j(\pi\delta f_i T)}\times\frac{\sin(\pi\delta f_i T)}{\pi\delta f_i T},\tag{6}$$

where the first factor originates from the phase of $r(t)r_0(t)^*$ at $t=t_0$, the second factor is the phase increased due to the integration in (4b), and the last factor represents the amplitude of $R(0,\delta f_i)$. Let T_i be the index i of the closest Doppler frequency hypothesis to the Doppler frequency of the incoming signal, then δf_{T_i} be the minimum frequency difference (i.e., $f_D^{T_i}$ is the closest Doppler frequency hypothesis to f_D) in the 2D search space and the correlation $R(0,\delta f_i)$ (6) for neighboring Doppler frequency hypotheses $f_D^{T_i\pm n}(=f_D^{T_i}\pm\ \triangle fn=f_D^{T_i}\pm\frac{n}{2T},n=1,2,3,...)$ can be expressed as

$$R(0,\delta f_{T_i\pm n})=e^{j(2\pi(\delta f_{T_i}\mp\frac{n}{2T})t_0+\theta)}\times e^{j(\pi\delta f_{T_i}T\mp\frac{1}{2}n\pi)}\times\frac{\sin(\pi\delta f_{T_i}T\mp\frac{n\pi}{2})}{\pi\delta f_{T_i}T\mp\frac{n\pi}{2}}.\tag{7}$$

Since δf_{T_i} is assumed to be small (i.e., $|\delta f_{T_i}|\le 0.5\triangle f$), $R(0,\delta f_{T_i\pm n})$ for $n\ge 2$ is negligible, and, therefore, only three consecutive Doppler frequencies f_D^i $(i=T_i-1,T_i,T_i+1)$ can deliver non-negligible signal energy. In a summary, when both $|\delta\tau_l|<T_c$ and $|\delta f_i T|<1$ are satisfied, a 2D hypothesis testing yields non-negligible mean value that represents a good portion of the incoming signal energy observed in the hypothesis testing. Note that there is a phase decrease of $\frac{n\pi}{2}$ in the second factor of $R(0,\delta f_{T_i\pm n})$ in (7) due to the increase of the Doppler frequency hypothesis by $\frac{n}{2T}$. Note also that when $t_0=0$ and the phase of $r_0(t)$ (2) is added by $\frac{n\pi}{2}$ in advance of the correlation (4a), the first and the second factors of $R(0,\delta f_{T_i\pm n})$ become the same for all n so that the resulting phase of $R(0,\delta f_{T_i\pm n})$ becomes the same for all Doppler frequency hypotheses.

III. Two-Dimensional Compressed Correlator

The TDCC makes use of the fact that a hypothesis testing with a code phase and a Doppler frequency next to the true hypothesis can yield a non-negligible amount of signal energy, and that the results of hypothesis testing with neighboring code phases and Doppler frequencies to the true hypothesis can be coherently combined. Fig. 2 shows the schematic diagram of the proposed TDCC that coherently accumulates most of the signal energy spread in $K_2=K_lK_i$ hypotheses (K_l code phases and K_i Doppler frequencies) around the true code phase and Doppler frequency of an incoming signal. The reset signal to K_i numerically controlled oscillators (NCO's) is applied at the beginning of the correlation to set the phase of all carrier signals at $t=t_0$ equal to zero. The sum of K_i carrier signals in Fig. 2 can be found as

$$f_0(t)=\sum_{p=0}^{K_i-1}\exp\Big[j2\pi(f_{IF}+f_D^i+p\triangle f)t-j\frac{p\pi}{2}\Big],\tag{8}$$

and the accumulated K_l PN code sequences in Fig. 2 is

$$s_0(t)=\sum_{m=0}^{K_l-1}P(t-K_l-m),\tag{9}$$

so that the complex TDCC ACF output $Z_I^1+jZ_Q^1$ can be expressed as

$$\begin{aligned}Z_I^1+jZ_Q^1&=\sum_{\{l,i\}}R(\delta\tau_l,\delta f_i)\\&=\frac{1}{T}\int_0^T\big[\big(h_L(t)*r(t)\big)f_0^*(t)\big]s_0(t)\,dt.\end{aligned}\tag{10}$$

Notice that the signal $f_0(t)$ can be pre-generated and its discrete-time samples can be stored in a memory so that the process in (10) can be implemented with a digital baseband processor, and that the phases of the K_i carrier signals are

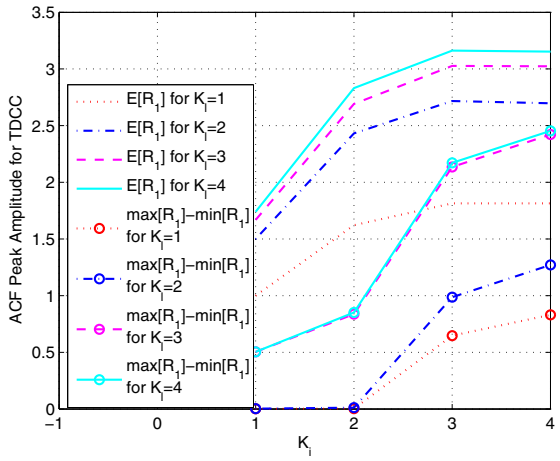

Fig. 3. Accumulated signal amplitudes for some K_l w.r.t. K_i.

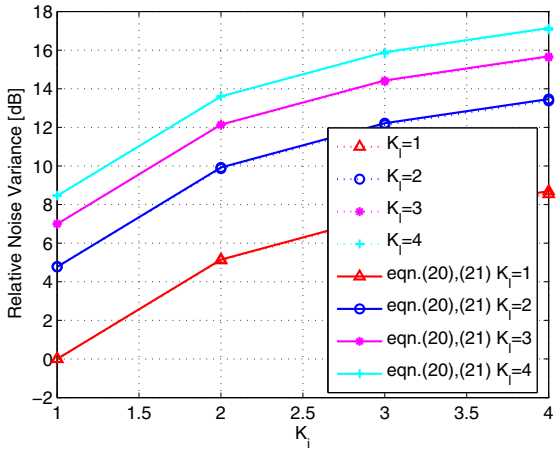

Fig. 4. V_1 for some K_l w.r.t. K_i.

compensated in advance by adding $\frac{p\pi}{2}$ as in (8) for the phase decrease due to the integration.

In practice, there is an unknown random frequency offset between the true Doppler frequency of the incoming signal f_D and the most correct Doppler frequency hypothesis $f_D^{T_i}$. The frequency offset has a uniform distribution in $[-\frac{1}{4T}, \frac{1}{4T}]$ for a receiver with a frequency search step size $\triangle f = \frac{1}{2T}$. If the frequency offset is assumed to be positive, the three most correct Doppler frequency hypotheses are expected to be at $f_D - \frac{3}{8T}$, $f_D + \frac{1}{8T}$, and $f_D + \frac{5}{8T}$, and the result of the three Doppler frequency hypothesis testings can be found from $R(0, \delta f_{T_i \pm n})$ (7) with $n = \{-1, 0, 1\}$ and $\delta f_{T_i} = 1/(8T)$. On the other hand, neglecting the effect of waveform shaping introduced by the low-pass filter $h_L(t)$ (3b), the ACF output $R(\delta\tau_l, 0)$ (5) has three non-zero consecutive mean values, $\frac{1}{2}$, 1, and $\frac{1}{2}$, at three code phase hypotheses around the true code phase for a receiver with $f_s = 2R_c$. Let T_l be the index of the most correct code phase hypothesis. Putting aside the phase rotation in the first and the second factors of $R(0, \cdot)$ in (7) as it can be manipulated and compensated using $f_0(t)$ (8), the amplitude of the ACF output $R(\delta\tau_l, \delta f_i)$ can be expressed in the discrete-time domain as

$$R[l,0] \simeq \begin{cases} 2^{-|l-T_l|} & |l-T_l| \le 1 \\ 0 & \text{otherwise,} \end{cases} \tag{11}$$

and

$$R[0,i] \simeq \begin{cases} \dfrac{8\sin(\frac{\pi}{8}[1+4(T_i-i)])}{[1+4(T_i-i)]\pi} & |i-T_i| \le 1 \\ 0 & \text{otherwise.} \end{cases} \tag{12}$$

From Fig. 1, and (11) and (12), it can be found that there are 9 neighboring hypotheses that contain signal energy when $f_s = 2R_c$ and $|\delta f_i T| = 0.5$.

Let the correct compressed hypothesis H_1^c be the coherently accumulated $K_2 (= K_l K_i)$ neighboring hypotheses that include the most correct individual hypothesis $H_1 = H(T_l, T_i)$. Depending on the size of K_l and K_i, and the relative location of H_1 within a small space made by the K_2 hypotheses, the resulting coherently accumulated TDCC ACF output R_1 can be expressed as

$$R_1 = \sum_{l \in S_l, i \in S_i} R[l,i], \tag{13}$$

where $S_l \in S_L = \{\{T_l - 1, T_l\}, \{T_l, T_l + 1\}, \{T_l - 1, T_l, T_l + 1\}\}$ and $S_i \in S_I = \{\{T_i - 1, T_i\}, \{T_i, T_i + 1\}, \{T_i - 1, T_i, T_i + 1\}\}$. Fig. 3 shows the expected value of R_1 (13) for random relative location of H_1 (i.e., $[T_l, T_i]$) within the K_2 hypotheses being tested by the TDCC. It also shows that both the mean difference between the maximum and the minimum of R_1 and the expected value of R_1 increase as K_2 increases in general. Note that when $K_l = 3$ and $3 \le K_i \le 4$, and assuming the signal energy in the most correct individual hypothesis be 1, the TDCC ACF output can yield a mean signal energy value about 9 $(= 3^2)$, and that the TDCC ACF output for $K_l = 2$ and $3 \le K_i \le 4$ can produce a mean signal energy value about 7.4 $(= 2.7^2)$. The mean difference between the maximum and the minimum of R_1 for $K_l = 3$ and $3 \le K_i \le 4$ is about 2.5 and for $K_l = 2$ and $3 \le K_i \le 4$ is about 1.25. Therefore the maximum signal energy contained in the incorrect compressed hypothesis is 0.75, 5/6, and 7/9 for $[K_l, K_i] = [2, 2]$, $[K_l, K_i] = [2, 3]$, and $[K_l, K_i] = [3, 3]$, respectively.

From (3b), the sum of noise in the complex TDCC ACF output $Z_I^1 + jZ_Q^1$ can be expressed using a complex expression

$$n^1(t) = \frac{1}{T}\int_0^T n(t) f_0^*(t) \sum_{l=0}^{K_l - 1} P(t - \tau_l)\, dt. \tag{14}$$

Since the three factors inside the integrand (14) are mutually independent, the variance of $n^1(t)$ can be obtained as

$$V_1 = \sigma_f^2 \sigma_P^2 f_s T N_0, \tag{15}$$

where σ_f^2 and σ_P^2 are the variance of the $f_0(t)$ (8) and $\sum_{l=0}^{K_l - 1} P(t - \tau_l)$, respectively. Since $f_s = 2R_c$, $P(t - \tau_{l+1}) = P(t - \tau_l - T_c/2)$, and $P[n] = P(n\frac{T_c}{2})$, therefore, when K_l is

odd

$$\sum_{l=0}^{K_l-1} P[n-\tau_l] = \begin{cases} P[n-\tau_0] + 2\sum_{l=1}^{\lfloor \frac{K_l}{2} \rfloor} P[n-\tau_{2l}], \\ \qquad \text{for } n \text{ odd} \\ 2\sum_{l=1}^{\lfloor \frac{K_l}{2} \rfloor} P[n-\tau_{2l-1}] + P[n-\tau_{K_l-1}], \\ \qquad \text{otherwise} \end{cases} \tag{16}$$

and when K_l is even,

$$\sum_{l=0}^{K_l-1} P[n-\tau_l] = \begin{cases} 2\sum_{l=1}^{\lfloor \frac{K_l}{2} \rfloor} P[n-\tau_{2l}] + \sum_{l\in\{0,K_l-1\}} P[n-\tau_l], \\ \qquad \text{for } n \text{ odd} \\ 2\sum_{l=1}^{\lfloor \frac{K_l}{2} \rfloor} P[n-\tau_{2l-1}], \\ \qquad \text{otherwise.} \end{cases} \tag{17}$$

From (16) and (17), it can be found that $\sigma_P^2 = 2K_l - 1$. Since

$$\begin{aligned} \frac{1}{T}\int_0^T |f_0(t)|^2 dt &= \frac{1}{T}\int_0^T \left| \sum_{n=0}^{K_i-1} e^{j(\frac{t}{T}-\frac{1}{2})n\pi} \right|^2 dt \\ &= K_i + \sum_{n=1}^{\lfloor \frac{K_i}{2} \rfloor} \frac{4(-1)^{n+1}(K_i-2n+1)}{(2n-1)\pi} \\ &\simeq 2K_i - 1, \end{aligned} \tag{18}$$

the variance of $n^1(t)$ can be found as

$$V_1 \simeq (2K_i - 1)(2K_l - 1) fsTN_0. \tag{19}$$

Fig. 4 shows an exact match between the $\sigma_f^2\sigma_P^2$ evaluated from 10^4 Monte Carlo simulations and the algebraic expressions. The simulation result shown in Fig. 4 is utilized to determine the decision thresholds of the 1st and 2nd stages to achieve a fixed false alarm rate in TDCC. When the 1st dwell search finds a $Z^1 (= (Z_I^1)^2 + (Z_Q^1)^2)$ larger than the 1st stage detection threshold γ_1, the code phase and Doppler frequency information $[l, i]$ of the current combined hypothesis is sent to the 2nd dwell search. Since there are K_2 individual hypotheses that constitute a combined hypothesis H^c, and K_2 is not very large, the 2nd dwell search is to find the most correct code phase and Doppler frequency hypothesis and can be realized with the conventional serial search technique that finds the maximum 2nd dwell search output $Z^2 (= (Z_I^2)^2 + (Z_Q^2)^2)$ larger than a detection threshold γ_2.

IV. Performance Analysis

The performance of the proposed technique can be analyzed using receiver operating characteristic (ROC) and mean acquisition time [12] for a given SNR of the decision variable Z^1 in Fig. 2. The SNR of $Z^1 = (Z_I^1)^2 + (Z_Q^1)^2$ can be defined as

$$\text{SNR}|_{Z^1} = 20\log_{10}\left(\frac{f_s T R_1}{\sqrt{V_1}}\right) \tag{20}$$

where $f_s T$ is the number of signal samples coherently accumulated for detection. The noise variances for I- and Q-channel ACF outputs (Z_I^1 and Z_Q^1, respectively) are the same to $V_1/2$. When the decision variable Z^1 is larger than the detection threshold γ_1 in the 1st dwell search, the indices $\{[l, i] | l \in S_l, i \in S_i\}$ of all hypotheses that constitute the compressed hypothesis H_1^c are transferred to the 2nd dwell search, where conventional search (i.e., a correlator with $K_l = K_i = 1$) is used for the given K_2 individual hypotheses. Let Z^2 denote the decision variable of the 2nd dwell search, then the SNR of Z^2 can be found from [12]

$$\text{SNR}|_{Z^2} = 20\log_{10}\left(\frac{f_s T R^f[0]}{\sqrt{V_2}}\right), \tag{21}$$

where

$$V_2 = f_s T N_0. \tag{22}$$

The decision variable Z^2 is then compared to the detection threshold γ_2 to find the most correct individual hypothesis. In practice, the comparison of Z^2 to γ_2 may result in detection of a hypothesis at $T_l \pm 1$ or $T_i \pm 1$, which is still within the accuracy tolerance for a PN code acquisition function and assumed a correct hypothesis detection in the following analysis.

When the current hypothesis is H_1^c (in the 1st dwell search) or H_1 (in the 2nd dwell search), the variable Z^i ($i = 1$ or 2, respectively) has a noncentral χ^2 distribution with two degrees of freedom

$$P_1(Z^i) = \frac{1}{V_i}\exp\left(\frac{-(Z^i + S_i^2)}{V_i}\right) I_0\left(\frac{2S_i\sqrt{Z^i}}{V_i}\right), \tag{23}$$

where $I_0(\cdot)$ is the zeroth-order modified Bessel function of the first kind, and $S_1 = f_s T R_1$ and $S_2 = f_s T R^f[0]$ are the signal amplitudes from the 1st and 2nd dwell searches, respectively. On the other hand, the variable Z^i ($i = 1$ or 2) has a central χ^2 distribution with two degrees of freedom when the current hypothesis is not H_1^c or H_1, respectively,

$$P_0(Z^i) = \frac{1}{V_i}\exp\left(\frac{-Z^i}{V_i}\right). \tag{24}$$

Using $P_1(Z^i)$ (23) and $P_0(Z^i)$ (24), the detection, miss, and false alarm probabilities in the i-th dwell search can be found in [12]

$$\begin{aligned} P_D^i &= \int_{\gamma_i}^{\infty} P_1(Z^i) dZ^i = \int_{\gamma_i/V_i}^{\infty} e^{-x+\mu_i} I_0(2\sqrt{\mu_i x}) dx \\ &= Q\left(S_i\sqrt{\frac{2}{V_i}}, \sqrt{\frac{2\gamma_i}{V_i}}\right) \end{aligned} \tag{25}$$

$$P_M^i = 1 - P_D^i \tag{26}$$

$$P_F^i = \int_{\gamma_i}^{\infty} P_0(Z^i) dZ^i = \exp\left(-\frac{\gamma_i}{V_i}\right), \tag{27}$$

respectively, where $\mu_i = \frac{S_i^2}{V_i}$ ($i = 1$ or 2) and $Q(a, b)$ is the Marcum's Q-function [18]. Fig. 5 shows ROC plots of the conventional correlator and the proposed technique applied to a receiver that has a chip rate $R_c = 1$MHz, 2MHz BPF bandwidth, sampling frequency $f_s = 2R_c$, and correlation length $T = T_0$ ($T_0 = 1$msec). The SNR described in the legend of Fig. 5 is the coherent SNR [4] (i.e., the SNR of the ACF output before squaring) of the conventional correlator with

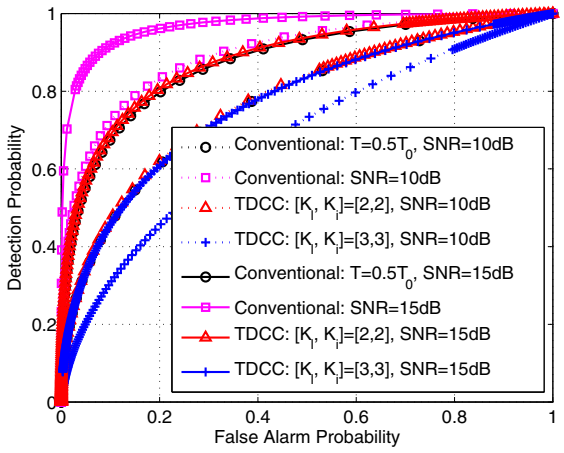

Fig. 5. Receiver operating characteristics.

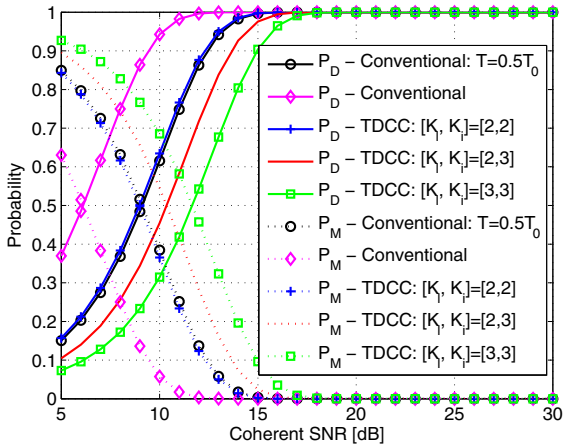

Fig. 6. Detection probability and miss detection probability ($P_F = 10^{-2}$).

$T = T_0$ (i.e., no hypothesis compression). As expected, the conventional correlator ACF output with $T = T_0$ is about 3dB higher than that with $T = 0.5T_0$, and the conventional correlator with $T = 0.5T_0$ has a very similar performance to the proposed TDCC with $[K_l, K_i] = [2, 2]$. In fact, the proposed TDCC with $[K_l, K_i] = [2, 2]$ has about 2.5dB gain loss in the ACF output comparing to the conventional correlator with $T = T_0$. However, the performance of the proposed TDCC degrades as $K_l K_i$ increases in Fig. 5. Fig. 6 shows the detection and miss detection probabilities of the conventional technique and the proposed TDCC with respect to the coherent SNR of the ACF output [4] for a conventional correlator when $P_F = 10^{-2}$. As expected, the detection and miss detection probabilities of the proposed TDCC technique with $[K_l, K_i] = [2, 2]$ is slightly better than those of the conventional correlator with $T = 0.5T_0$, but the performance of the proposed TDCC technique degrades as $K_i K_l$ increases.

Fig. 7 shows the circular search state diagram of the proposed technique. If current compressed hypothesis H^c being tested by the proposed TDCC is H_1^c (i.e., $H^c = H_1^c$), the hypothesis testing may have a successful signal detection with probability P_D^1 or miss the signal detection with probability P_M^1. On the other hand, if $H^c = H_0^c$ (incorrect compressed

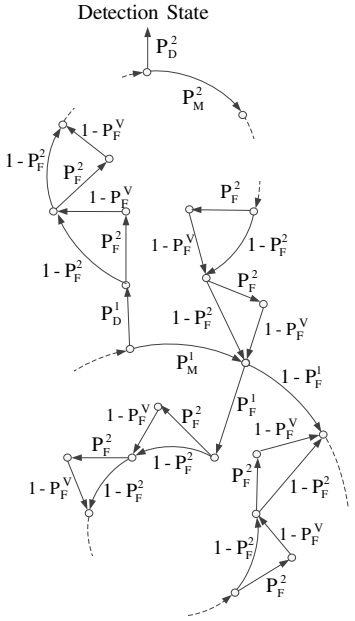

Fig. 7. Circular state diagram.

hypothesis), it may conclude the absence of signal with probability $1-P_D^1$ or may result in a false alarm with probability P_F^1. When the TDCC declares a signal detection at $H^c = H_1^c$, the search algorithm proceeds to the 2nd dwell search, where a conventional correlator (i.e., $K_l = K_i = 1$) based technique is applied to test the K_2 $(= K_l K_i)$ individual hypotheses from the H_1^c. If the individual hypothesis H being tested is the correct hypothesis (i.e., $H = H_1$), the 2nd dwell search may have a successful signal detection with probability P_D^2 or miss the signal detection with probability P_M^2. If $H = H_0$ (incorrect hypothesis), it may conclude the absence of signal with probability $1-P_F^2$ or a false alarm with probability P_F^2. When a signal detection is declared or a false alarm is made in the 2nd dwell search, the acquisition function needs to proceed to the verification mode that can take T^p seconds long. We assume that the hypothesis testing in the verification mode is always successful so that $P_D^V = 1$ and $P_F^V = 0$ in the following analysis. As shown in Fig. 7, the correct hypothesis detection starts with signal detection in the 1st dwell search at $H^c = H_1^c$. The 2nd dwell search needs to test all K_2 hypotheses, one of which is the correct hypothesis $H = H_1$. The overall branch transfer function for the correct hypothesis detection can be expressed as

$$H_D(T) = P_D^1 P_D^2 T^2 \frac{1}{K_2} \sum_{r=0}^{K_2-1} \left[(1-P_F^2)T + P_F^2 T^{p+1}\right]^r = \frac{(1-[(1-P_F^2)T + P_F^2 T^{1+p}]^{K_2}) P_D^1 P_D^2 T^2}{K_2(1-[(1-P_F^2)T + P_F^2 T^{1+p}])}. \quad (28)$$

The overall correct hypothesis missed occurs when signal detection is missed in the 1st dwell, or when the signal detection in the 1st dwell search is successful but missed in the 2nd dwell search. Therefore, the overall branch transfer function for the correct hypothesis missed can be found as

$$H_M(T) = P_M^1 T + P_D^1 P_M^2 T^2 [(1-P_F^2)T + P_F^2 T^{1+p}]^{K_2-1} \quad (29)$$

The incorrect hypothesis branch comes from an incorrect hypothesis node to the next node, and when a false alarm occurs in the 1st dwell search, the 2nd dwell search needs to test all K_2 individual hypotheses. Therefore, the overall branch transfer function for incorrect hypothesis can be

$$H_0(T) = (1-P_F^1)T + P_F^1 T[(1-P_F^2)T + P_F^2 T^{1+p}]^{K_2}. \quad (30)$$

Denoting K_1 the total number of compressed hypotheses in the 1st dwell search (i.e., K_1K_2 is the total number of individual hypotheses in the entire 2D search space), the overall transfer function of the proposed double dwell acquisition system can be expressed as [12] and [19]

$$H(T) = \frac{H_D(T)[1-H_0^{K_1-1}(T)]}{K_1[1-H_0(T)][1-H_M(T)H_0^{K_1-1}(T)]}, \quad (31)$$

and using (28), (29), and (30), the mean acquisition time (MAT) can be obtained after some algebraic manipulations as

$$\begin{aligned}\mu_T &= \left.\frac{dH(T)}{dT}\right|_{T=1} \times T \\ &= \frac{(K_1-1)P_D^1P_D^2T}{K_1(1-H_M(1))}\left[\frac{K_1+2}{2}\right. \\ &\quad + \frac{1+pP_F^2}{2}\left(K_2\left[1+(K_1-2)P_F^1\right]-1\right) \\ &\quad + \frac{1}{1-H_M(1)}\left(P_M^1+P_M^2P_D^1\left[(K_2-1)(1+pP_F^2)+2\right]\right. \\ &\quad \left.\left. + (P_M^1+P_M^2P_D^1)(K_1-1)\left[1+K_2P_F^1(1+pP_F^2)\right]\right)\right], \quad (32)\end{aligned}$$

where $H_M(1) = P_M^1 + P_M^2P_D^1$. The variance of acquisition time (VAT) can be obtained using the following equation

$$\sigma_T^2 = \left(\frac{d^2H(T)}{dT^2} + \frac{dH(T)}{dT}\left[1 - \frac{dH(T)}{dT}\right]\right)\Bigg|_{T=1} \times T^2. \quad (33)$$

For high SNR, it is obvious that $P_M^1 \to 0$, $P_M^2 \to 0$, $P_F^1 \to 0$, $P_F^2 \to 0$, $H_M(1) \to 0$, $P_D^1 \to 1$, and $P_D^2 \to 1$, and, as a result,

$$\mu_T\big|_{\text{SNR}\uparrow} = \frac{(K_1-1)(K_1+K_2+1)T}{2K_1}. \quad (34)$$

Similarly, the VAT for high SNR is

$$\begin{aligned}\sigma_T^2\big|_{\text{SNR}\uparrow} = \frac{(K_1-1)}{12K_1^2} \times (&K_1^3 - 17K_1^2 + 3K_2^2 + K_1K_2^2 + \\ &24K_1K_2 + 9K_1 + 6K_2 + 3)T^2. \quad (35)\end{aligned}$$

V. Practical Issues

A. Sensitivity Improvement

Similarly to the conventional correlator based techniques, the proposed technique can improve detection sensitivity by increasing the coherent correlation length T and by applying non-coherent accumulation technique. Obviously from (20) and (21), increasing T results in an increase of SNR in both the 1st and the 2nd dwell searches. Let Z_l^i ($i=1$ or 2) be the decision variable obtained in the i-th dwell search at $t = lT$, and Z_L^i ($i=1$ or 2) be the L times non-coherently accumulated decision variable of Z_l^i. Assuming the L decision variables Z_l^i ($l = 1, 2, \ldots, L$) are independent, the probability distribution function of Z_L^i can be determined by finding the Laplace transform of $P_1(Z^i)$ (or $P_0(Z^i)$), taking L-th power of the Laplace transform, and inverting the transform as in [12]

$$\begin{aligned}P_1(Z_L^i) = \frac{1}{V_i}\left(\frac{Z_L^i}{LS_i^2}\right)^{\frac{L-1}{2}} &\exp\left(\frac{-(Z_L^i+LS_i^2)}{V_i}\right) \\ &\times I_{L-1}\left(\frac{2S_i\sqrt{LZ_L^i}}{V_i}\right) \quad (36)\end{aligned}$$

$$P_0(Z_L^i) = \frac{(Z_L^i)^{L-1}}{(L-1)!V_i^L}\exp\left(\frac{-Z_L^i}{V_i}\right), \quad (37)$$

where $i = 1, 2$ and $I_{L-1}(\cdot)$ is the $(L-1)$-th order modified Bessel function of the first kind. The resulting probabilities of detection, false alarm, and miss can be found as in [20]

$$P_D^i = Q\left(S_i\sqrt{\frac{2L}{V_i}}, \sqrt{\frac{2\gamma_i}{V_i}}\right) \quad (38)$$

$$P_F^i = \exp\left(-\frac{\gamma_i}{V_i}\right)\sum_{l=0}^{L-1}\frac{1}{l!}\left(\frac{\gamma_i}{V_i}\right)^l, \quad (39)$$

$$P_M^i = 1 - P_D^i, \quad (40)$$

respectively, where $i=1$ and 2.

B. Hardware Complexity

Fig. 2 shows that the schematic diagram of the proposed TDCC. The compressed code phase signal generation block in Fig. 2 requires multiple delay components and a summation block to combine the generated PRN codes with different delays. The multiplication between the received signal $r_0(t)$ and the compressed code phase signal $s_0(t)$ may require a multiplier, while the conventional correlator may just require sign changes of the received signal samples depending on the instantaneous value of the receiver generated PRN code. At the same time, there is more hardware required to generate compressed Doppler frequency signal $f_0(t)$ with multiple Doppler frequencies. For example, as shown in Fig. 2, the number of NCO should be increased linearly with K_i, and a phase compensation block and a summation block are necessary. However, in practice, when K_i is large (e.g., larger than 2), the compressed Doppler frequency signal $f_0(t)$ can be pre-generated and stored in a memory block and can be used in real-time.

C. Detection Threshold

There a number of ways to determine the detection threshold γ_1 and γ_2. In [13], the detection threshold is determined from numerous Monte Carlo simulations to yield the minimum MAT, and, in practice, the detection threshold is determined by calculating the noise variance from the correlator output in order to fix or maintain the false alarm rate to a very small value [21] and [22]. On the other hand, in [23], optimal the 1st and the 2nd stage thresholds are found from a solution of optimization problem with probability variables. In the following section, we exploit the noise variance observed from the TDCC output to find an appropriate detection threshold to maintain a constant false alarm rate (CFAR).

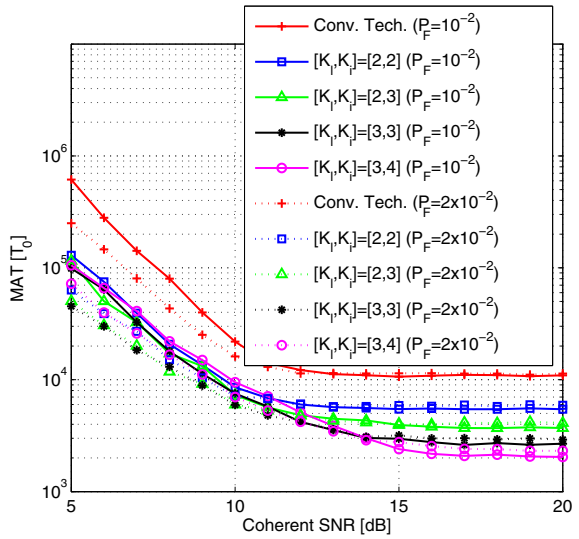

Fig. 8. Monte Carlo simulation results for the MAT.

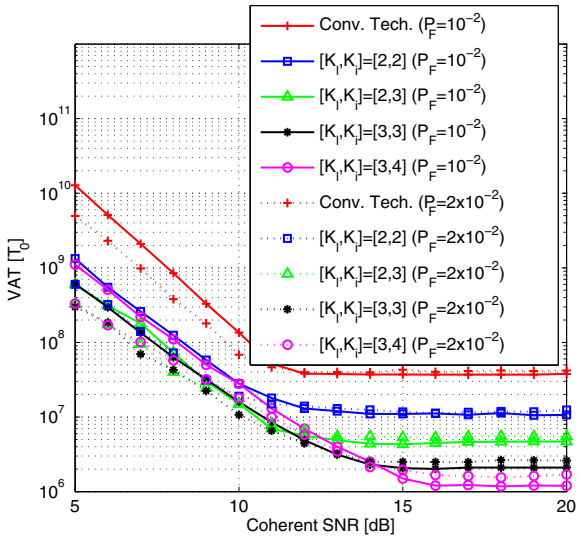

Fig. 9. Monte Carlo simulation results for the VAT.

VI. Numerical Results

In this section, the proposed technique is tested for a receiver with 2MHz BPF bandwidth, sampling frequency $f_s = 2R_c$, correlation length $T = T_0$(1msec), and code phase and Doppler frequency search step sizes $0.5T_c$ and $\Delta f = 500$Hz, respectively, trying to acquire an incoming PN code signal that has a chip rate $R_c = 1$MHz and an unknown Doppler frequency at somewhere between -5KHz and 5KHz. The 1st stage detection threshold γ_1 is determined adaptively to the variation of noise variance so that the the 1st stage can have a CFAR [21]. Since the proposed TDCC may have different noise variance in the ACF output depending on K_l and K_i, the noise variance and the detection threshold are a function of K_l and K_i. In the following simulations, the target CFAR is set to 10^{-2} and 2×10^{-2}, and the detection threshold γ_i for the i-th dwell search is set from P_F^i (27) as

$$\gamma_i = -V_i \log(P_F^i). \tag{41}$$

Fig. 8 shows a result obtained from 10^4 Monte Carlo simulations performed to evaluate the MAT of the proposed technique for various K_l and K_i and to compare with the conventional correlator based double dwell search technique that has the 1st and the 2nd dwell search correlation length $T = 0.5T_0$ and $T = T_0$, respectively. The horizontal axis is the coherent SNR of the ACF output obtained with a conventional correlator with $T = T_0$. The proposed technique employs TDCC in the 1st dwell search and a conventional correlator based search in the 2nd dwell search, where $T = T_0$ for both dwell searches. As shown, the proposed technique has 2$\sim$5 times smaller MAT than the conventional double dwell search technique when SNR is high enough (> 18dB), and the MAT decreases as $K_l K_i$ increases due to the increase of noise variance V_1 (19). It can be found that the proposed technique with $P_F = 0.01$ has about 50%, 67%, 78%, or 83% less MAT than the conventional double dwell search technique for $[K_l, K_i] = [2, 2]$, $[K_l, K_i] = [2, 3]$, $[K_l, K_i] = [3, 3]$, or $[K_l, K_i] = [3, 4]$, respectively. The decrease of MAT for high SNR is as expected, since the total number of compressed hypothesis to test is $K_l K_i$ times smaller than the total number of individual hypothesis to test for a serial search technique, and the conventional double dwell search technique saves 50% of MAT, since it has $T = 0.5T_0$ in the first dwell search. On the contrary, as the SNR decreases down below 18dB, the MAT of the proposed technique with larger $K_l K_i$ starts to increase at higher SNR. Even for low SNR (< 15dB), the proposed technique has at least 50% less MAT than the conventional double dwell search technique. Fig. 9 shows a result of 10^4 Monte Carlo simulations performed to evaluate the VAT (Variance of Acquisition Time) of the proposed technique for various K_l and K_i and to compare with the conventional correlator based double dwell search technique that has the 1st and the 2nd dwell search correlation length $T = 0.5T_0$ and $T = T_0$, respectively. The overall VAT plots in Fig. 9 have very similar pattern to the MAT plots in Fig. 8; VAT decreases as $K_l K_i$ increases for SNR higher than 18dB, the proposed technique with larger $K_l K_i$ has higher SNR point below which VAT increases rapidly; for high SNR (> 18dB), the proposed technique with $P_F = 0.01$ has about 75%, 89%, 95%, or 98% less VAT than the conventional double dwell search technique when $[K_l, K_i] = [2, 2]$, $[K_l, K_i] = [2, 3]$, $[K_l, K_i] = [3, 3]$, or $[K_l, K_i] = [3, 4]$, respectively. Even for low SNR (< 15dB), the proposed technique has at least 80% less VAT than the conventional double dwell search technique. As shown in Fig. 8 and Fig. 9, the increase of P_F (equivalently, the decrease of γ_i) results in the increase of both MAT and VAT in high SNR (> 18dB) but the decrease of both MAT and VAT in low SNR (< 10dB). This opposite tendency is due to the fact that the increase of detection probability is negligibly small in the high SNR but not negligibly small in the low SNR for the decrease of γ_i. Note that, in all cases, the MAT and the VAT increase rapidly as the SNR decreases down below 13dB, for which the receiver may need to increase the coherent integration length T or the number of non-coherent accumulation as discussed in Section V. Note also that the MAT and VAT of the proposed technique are much smaller than those of the conventional double dwell search technique.

VII. Conclusion

A novel double dwell search technique, for BPSK DSS signals, that uses the TDCC in the 1st dwell search and the conventional correlator in the 2nd dwell search has been proposed. The performance of the proposed technique has been analyzed and its performance has been compared to the conventional double dwell search technique [12]. It has been shown that the proposed technique has strong advantages over the conventional double dwell search technique; the proposed technique has at least 50% less MAT and 75% less VAT than the conventional double dwell search technique for any $K_l, K_i > 2$ when SNR is good enough, and the proposed technique has much smaller MAT and VAT even at low SNR. In this paper, CFAR is used to set the false alarm probability to a fixed value and find the performance of the proposed technique and the conventional technique. However, the performance of the proposed technique can be further improved using the optimum choice of the false alarm probability [23].

References

[1] B. Parkinson, J. Spilker, P. Axelrad, and P. Enge, Eds. "GPS Receivers," in *Gobal Positioning System: Theory and Applications*. American Institute of Aeronautics and Astronautics, 1996, pp. 329–405.

[2] P. Misra and P. Enge, "Signal Conditioning and Acquisition," in *Gobal Positioning System: Signals, Measurements, and Performance*, 2nd ed. Ganga-Jamuna Press, 2006, pp. 431-466.

[3] P. W. Ward, "GPS receiver search techniques," in *Proc. 1996 ION PLANS*, pp. 604–611.

[4] F. Van Diggelen, "Assistance, the 'A' in A-GPS," in *A-GPS: Assisted GPS, GNSS, and SBAS*. Artech House, 2009. pp. 31-60.

[5] H. Li, M. Lu, X. Cui, and Z. Feng "Generalized zero-padding scheme for direct GPS P-code acquisition," *IEEE Trans. Wireless Commun.*, vol. 8, no. 6, pp. 2866–2871, June 2009.

[6] Y. Huang and J. Wang, "Rapid search methods for code acquisition in UWB impulse radio communications," *IEEE Trans. Wireless Commun.*, vol. 6, no. 10, pp. 3578–3588, Oct. 2007.

[7] L. Reggiani and G. M. Maggio, "Rapid search methods for code acquisition in UWB impulse radio communications," *IEEE J. Sel. Areas Commun.*, vol. 23, no. 5, pp. 898–908, May 2005.

[8] K. M. Chugg and M. Zhu, "A new approach to rapid PN code acquisition using iterative message passing techniques," *IEEE J. Sel. Areas Commun.*, vol. 23, no. 5, pp. 884–897, May 2005.

[9] Y. H. Lee and S. Tantaratana, "Sequential acquisition of PN sequences for DS/SS communications: design and performance," *IEEE J. Sel. Areas Commun.*, vol. 10, no. 4, pp. 750–759, May 1992.

[10] Y. H. Lee and S. J. Kim, "Sequence acquisition of DS-CDMA systems employing gold sequences," *IEEE Trans. Veh. Technol.*, vol. 49, no. 6, pp. 2397–2404, Nov. 2000.

[11] J. Ibrahim and R. M. Buehrer, "Two-stage acquisition for UWB in dense multipath," *IEEE J. Sel. Areas Commun.*, vol. 24, no. 4, pp. 801–807, Apr. 2006.

[12] A. J. Viterbi, "Synchronization of Pseudorandom Signals," in *CDMA: Principles of Spread Spectrum Communication*. Addison-Wesley Publishing Company, 1995, pp. 39–75.

[13] E. A. Sourour and S. C. Gupta, "Direct-sequence spread-spectrum parallel acquisition in a fading mobile channel," *IEEE Trans. Commun.*, vol. 38, no. 7, pp. 992–998, July 1990.

[14] D. Akopian,"Fast FFT based GPS satellite acquisition methods," *IEE Proc.-Radar Sonar Navig.*, vol. 152, no. 4, Aug. 2005.

[15] C. Yang, J. Vasquez, and J. Chaffee, "Fast direct P(Y)-code acquisition using XFAST," in *Proc. 1999 ION GPS*, pp. 317–324.

[16] H. Li, X. Cui, M. Lu, and Z. Feng "Dual-folding based rapid search method for long PN-code acquisition," *IEEE Trans. Wireless Commun.*, vol. 7, no. 12, pp. 5286–5296, Dec. 2008.

[17] S.-H. Kong, "A deterministic compressed GNSS acquisition technique," *IEEE Trans. Veh. Technol.*, vol. 62, no. 2, pp. 511–521, Feb. 2013.

[18] J. I. Marcum, *A Table of Q-functions*, Rand Corp. Report, RM-339, Jan. 1950.

[19] M. A. Abu-Rgheff, "Time Synchronization of Spread-Spectrum Systems," in *Introduction to CDMA Wireless Communications*. Academic Press, 2007, pp. 195-250.

[20] C. O'Driscoll, M. G. Petovello, and G. Lachapelle, "Software receiver strategies for the acquisition and re-acquisition of weak GPS signals," in *Proc. 2008 ION ITM*, pp. 843–854.

[21] Z. Ye, G. Memik and J. Grosspietsch "Energy detection using estimated noise variance for spectrum sensing in cognitive radio networks," in *Proc. 2008 WCNC*, pp. 711–716.

[22] E. D. Kaplan and C. J. Hegarty "Satellite signal acquisition, tracking, and data demodulation," in *Understanding GPS: Principles and Applications*, 2nd ed. Artech House, 2006, pp. 153-240.

[23] G. Giunta, A. Neri, and M. Carli "Constrained optimization of noncoherent serial acquisition of spread- spectrum code by exploiting the generalized Q-functions," *IEEE Trans. Veh. Technol.*, vol. 52, no. 5, pp. 1378–1385, Sept. 2003

Seung-Hyun Kong (M'06) received a B.S.E.E. from the Sogang University, Korea, in 1992, an M.S.E.E. from the Polytechnic University, New York, in 1994, and a Ph.D. degree in Aeronautics and Astronautics from Stanford University, CA, in 2006. From 1997 to 2004, he was with Samsung Electronics Inc. and Nexpilot Inc., both in Korea, where his research focus was on wireless communication systems and mobile positioning technologies. In 2006, he was involved with hybrid positioning technology development using wireless location signature and Assisted GNSS at Polaris Wireless, Inc., Santa Clara, and from 2007 to 2009, he was a research staff at Corporate R&D of Qualcomm Inc., San Diego, where his R&D focus was on the indoor location technologies and advanced GNSS technologies. Since 2010, he has been an Assistant Professor at The CCS Graduate School for Green Transportation in the Korea Advanced Institute of Science and Technology (KAIST). His research interests include super-resolution signal processing, detection and estimation for navigation systems, and vehicular communication systems.

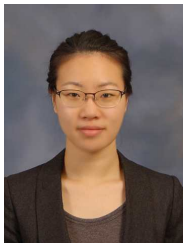

Binhee Kim (S'08) received a B.S.E.E.and M.S.E.E. from the Korea Advanced Institute of Science and Technology (KAIST), Korea, in 2008 and 2010, respectively. She is currently pursuing the Ph.D. degree at the CCS Graduate School for Green Transportation in the KAIST. Her research interests include super-resolution signal processing, detection and estimation for navigation systems.